PNAS RESEARCH ARTICLE | BIOPHYSICS AND COMPUTATIONAL BIOLOGY OPEN ACCESS

# Structural determinants of protein kinase A essential for CFTR channel activation

Csaba Mihályi[a,b,c,1], Iordan Iordanov[a,b,c,1], Andras Szollosi[a,b,c], and László Csanády[a,b,c,2]

Affiliations are included on p. 11.

Edited by Susan Taylor, University of California, San Diego, La Jolla, CA; received April 17, 2024; accepted September 30, 2024

**Cystic Fibrosis Transmembrane Conductance Regulator (CFTR), the anion channel mutated in cystic fibrosis (CF) patients, is activated by the catalytic subunit of protein kinase A (PKA-C). PKA-C activates CFTR both noncatalytically, through binding, and catalytically, through phosphorylation of multiple serines in CFTR's regulatory (R) domain. Here, we identify key molecular determinants of the CFTR/PKA-C interaction essential for these processes. By comparing CFTR current activation in the presence of ATP or an ATP analog unsuitable for phosphotransfer, as well as pseudosubstrate peptides of various lengths, we identify two distinct specific regions of the PKA-C surface which interact with CFTR to cause noncatalytic and catalytic CFTR stimulation, respectively. Whereas the "substrate site" mediates CFTR phosphorylation, a distinct hydrophobic patch (the "docking site") is responsible for noncatalytic CFTR activation, achieved by stabilizing the R domain in a "released" conformation permissive to channel gating. Furthermore, by comparing PKA-C variants with different posttranslational modification patterns, we find that direct membrane tethering of the kinase through its N-terminal myristoyl group is an unappreciated fundamental requirement for CFTR activation: PKA-C demyristoylation abolishes noncatalytic, and profoundly slows catalytic, CFTR stimulation. For the F508del CFTR mutant, present in ~90% of CF patients, maximal activation by demyristoylated PKA-C is reduced by ~10-fold compared to that by myristoylated PKA-C. Finally, in bacterial genera that contain common CF pathogens, we identify virulence factors that demyristoylate PKA-C in vitro, raising the possibility that during recurrent bacterial infections in CF patients, PKA-C demyristoylation may contribute to the exacerbation of lung disease.**

cystic fibrosis | cAMP-dependent protein kinase | PKI peptide | N-myristoylation | IpaJ

## Significance

The CFTR anion channel mediates salt-water transport across epithelia and is activated by a kinase (PKA-C). Reduced activity of mutant CFTR causes cystic fibrosis (CF), and CFTR hyperstimulation by sustained PKA-C activity causes diarrhea. PKA-C activates CFTR noncatalytically, through binding, and catalytically, by phosphorylating the channel. We uncover important structural requirements for these two processes. First, two distinct PKA-C surface areas mediate noncatalytic and catalytic CFTR activation. Second, membrane anchoring of PKA-C through a covalently linked fatty (myristic) acid is required for both effects. We identify bacterial enzymes that cleave the myristic acid from PKA-C, thereby greatly reducing activation of mutant CFTR channels. That process might worsen disease symptoms in CF patients during lung infections.

The devastating disease cystic fibrosis (CF) is caused by mutations of the Cystic Fibrosis Transmembrane Conductance Regulator (CFTR), an anion channel expressed in the epithelia of the lung, the pancreas, and the gut, and regulated through phosphorylation by cAMP-dependent protein kinase (protein kinase A, PKA). Defects in the regulation of CFTR by PKA contribute to multiple disease pathologies. On the one hand, CFTR hyperstimulation by sustained PKA activity in the intestinal or renal epithelium, respectively, underlies excessive intestinal fluid loss in cholera and other secretory diarrheas (1), as well as progressive renal cyst growth in autosomal dominant polycystic kidney disease (ADPKD) (2). Clinical trials targeting the PKA pathway proved beneficial for the treatment of ADPKD (3). On the other hand, profoundly impaired phosphorylation by PKA exacerbates the consequences of protein processing/channel gating defects caused by the most common CF-associated CFTR mutations ΔF508 (4) and G551D (5). Moreover, although for most CF patients a combination of corrector (to stimulate CFTR protein processing) and potentiator drugs (to stimulate CFTR channel gating) provides significant symptomatic improvement (6), the potentiating effect of the only FDA-approved potentiator VX-770 is entirely dependent on CFTR channel phosphorylation (7). Pulmonary exacerbations, caused by recurrent lung infections, remain an important challenge in CF care: despite effective pharmacotherapy, for a large fraction of patients, eventual bacterial colonization of the lung by *Pseudomonas aeruginosa* or other pathogenic strains can still not be prevented (8).

CFTR is an ATP Binding Cassette (ABC) protein with an anion-selective pore formed by two transmembrane domains (TMD1, 2; Fig. 1*A*, *gray*) and gated by an ATP hydrolysis cycle at two cytosolic nucleotide binding domains (NBD1, 2; Fig. 1*A*, *blue* and *green*) (9). Formation of a tight NBD1-NBD2 dimer upon ATP binding opens the pore (10), and disruption of the tight dimer following ATP hydrolysis closes it (11, 12). The two ABC-typical halves of CFTR are linked by a unique cytosolic regulatory (R) domain (Fig. 1*A*, *red ribbon*) which inhibits channel opening unless it is phosphorylated at multiple serines by PKA (13, 14).

Author contributions: C.M., I.I., A.S., and L.C. designed research; C.M., I.I., A.S., and L.C. performed research; I.I., A.S., and L.C. contributed new reagents/analytic tools; C.M., I.I., A.S., and L.C. analyzed data; and C.M., I.I., A.S., and L.C. wrote the paper.

The authors declare no competing interest.

This article is a PNAS Direct Submission.



[1]C.M. and I.I. contributed equally to this work.

[2]To whom correspondence may be addressed. Email: csanady.laszlo@semmelweis.hu.

This article contains supporting information online at https://www.pnas.org/lookup/suppl/doi:10.1073/pnas.2407728121/-/DCSupplemental.

Published November 4, 2024.

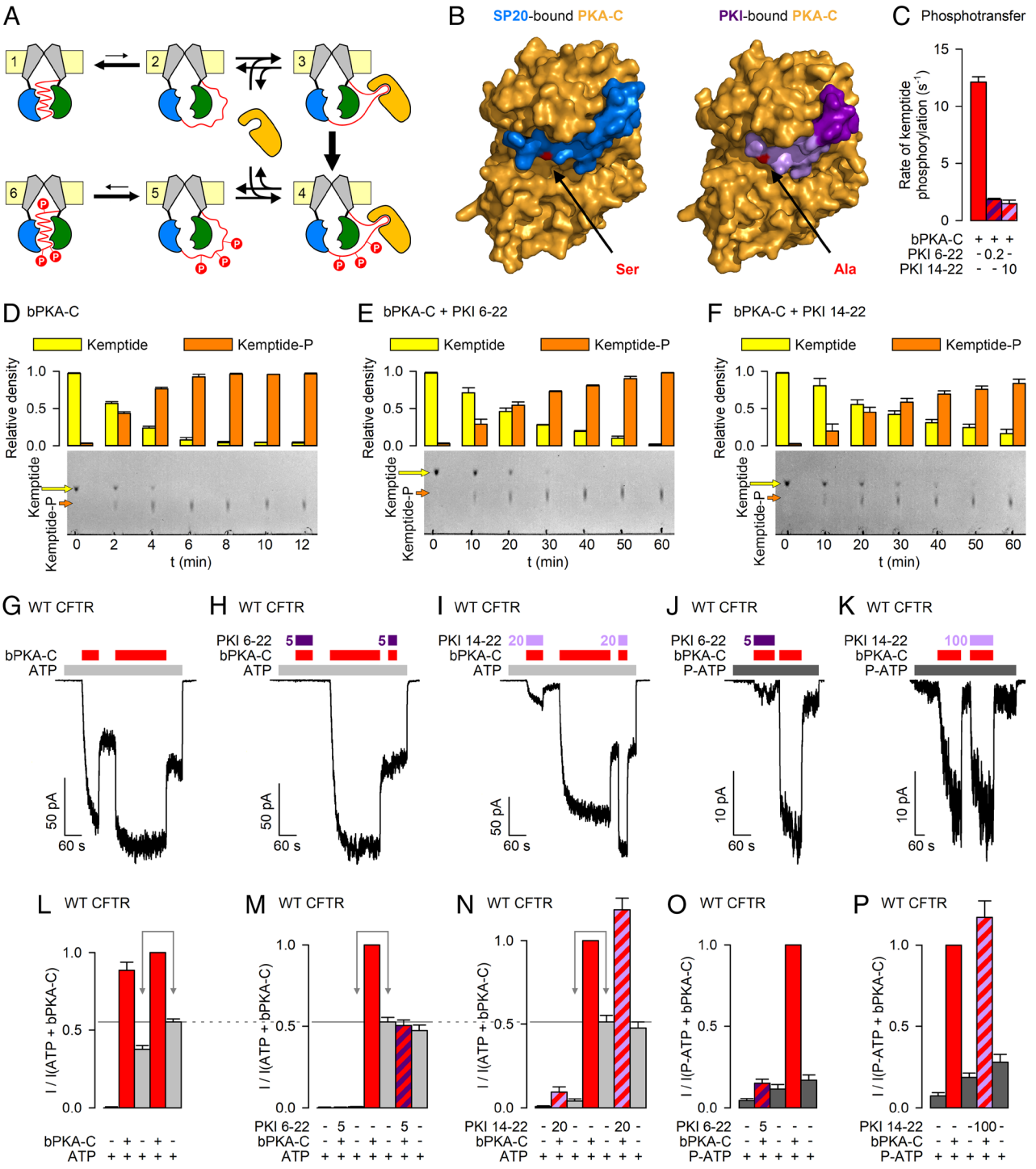


**Fig. 1.** Distinct regions of the PKA-C substrate binding cleft mediate noncatalytic and catalytic CFTR activation. (*A*) Cartoon representation of the kinetic scheme that describes CFTR channel activation. NBD1, *blue*; NBD2, *green*; TMD1 and TMD2, *gray*; R domain, *red ribbon*; phosphate groups, *red circles, P*; membrane, *yellow*; PKA-C, *orange*. States 1 to 6 represent only the possible states of the R domain: in states 2 to 5, ATP binding may induce NBD dimerization coupled to pore opening (not depicted). (*B*) Surface representations of PKA-C crystal structures with bound (*Left*, PDBID: 4O22) peptide substrate (SP20) or (*Right*, PDBID: 2GFC) inhibitor (PKI(5-24), only residues 6–22 shown). PKA-C, *orange*; SP20, *blue*; PKI residues 6–13, *dark purple*, PKI residues 14–22, *light purple*; target serine in SP20 and corresponding alanine in PKI, *red*. (*C*) Estimated $k_{cat}$ ($s^{-1}$) for bPKA-C without PKI peptides, with 0.2 μM PKI(6-22)amide, or with 10 μM PKI(14-22)amide, calculated from the data in *D–F*. (*D–F*) (*Bottom*) Time courses of kemptide phosphorylation resolved on TLC sheets. 5 nM bPKA-C without PKI (*D*), with 0.2 μM PKI(6-22)amide (*E*), or with 10 μM PKI(14-22)amide (*F*) were incubated with 20 μM TAMRA-kemptide + 200 μM MgATP for the indicated amounts of time at room temperature. *Upper row of spots*, dephospho-peptide; *lower row of spots*, phospho-peptide. (*Top*) Densitometric analysis of the TLC sheets. *Yellow* and *orange columns* plot fractional densities of the spots corresponding to the dephospho- and phospho-peptide, respectively. Data in *C–F* represent mean ± SEM, n = 3. (*G–K*) Macroscopic currents through inside-out patches excised from *Xenopus laevis* oocytes injected with cRNA for WT CFTR. Channels are activated by repeated exposures to 300 nM bPKA-C (*red bars*) in the presence of either 2 mM ATP (*G–I*; *light gray bars*) or 10 μM P-ATP (*J–K*; *dark gray bars*), with or without PKI(6-22)amide (*H* and *J*; *dark purple bars*) or PKI(14-22)amide (*I* and *K*; *light purple bars*). Colored numbers indicate PKI concentrations in μM. Membrane voltage was −40 mV. (*L–P*) Steady-state currents in the sequential segments of the experiment in the panel above, normalized to that in the presence of ATP+bPKA−C or P−ATP+bPKA−C [*red column* (*L*; *2nd red column*)]. In *L–N*, the ratios of the two *gray columns* marked by the *double arrows* report fractional CFTR phosphorylation after 1 min in 300 nM bPKA-C without PKI peptides (*L*), with 5 μM PKI(6-22)amide (*M*), or with 20 μM PKI(14-22)amide (*N*). *Horizontal gray lines* in *L–N* mark the quasi-maximal fractional contribution of the irreversible current component, reached after 3 min in 300 nM bPKA-C. Data in *L–P* represent mean ± SEM, n = 7 to 11 (*L–O*), n = 4 (*P*).

Because in living cells, CFTR's NBDs are continuously exposed to a saturating ATP concentration, physiological regulation of CFTR activity is realized through R-domain phosphorylation which tightly links the rate of transepithelial anion transport to cytosolic cAMP levels. The PKA holoenzyme consists of two regulatory (R) and two catalytic (C) subunits. Binding to an R subunit keeps the C subunit inactive. When cellular cAMP levels rise, the R subunits bind cAMP and release the C subunits (PKA-C) in free active form, allowing them to bind and phosphorylate their targets (15). PKA-C is a small (~350 a.a.) soluble protein that is subject to several posttranslational modifications. It is cotranslationally myristoylated at its N terminus (16) and autophosphorylated at several positions (17).

Despite its prime importance in physiology and disease, little is known about the molecular details of the CFTR/PKA-C interaction. The CFTR R domain is largely unstructured (18) and may adopt two major conformations that are at equilibrium with each other. In its "wedged-in" form, it is intercalated between the two NBDs preventing NBD dimerization and pore opening [(19, 20); Fig. 1*A*, states 1 and 6]; in its "released" form [(21, 22); Fig. 1*A*, states 2 to 5], it allows NBD dimerization and pore opening in response to ATP binding. Whereas for the unphosphorylated R domain, the equilibrium is heavily biased toward wedged-in (state 1 vs. 2), for the phosphorylated R domain, it is shifted toward released (state 5 vs. 6). Thus, phosphorylation causes "irreversible" CFTR stimulation, terminated only through the action of phosphatases. In addition, simple binding of PKA-C to CFTR can also keep the R domain released, causing additional, "rapidly reversible" stimulation for both unphosphorylated and phosphorylated CFTR [(23); Fig. 1*A*, states 3 and 4]. However, the structural interactions that underlie activation of CFTR by PKA-C are unknown. In the present study, we identify key molecular determinants of the CFTR/PKA-C interaction required for noncatalytic and catalytic CFTR stimulation, respectively.

## Results

**Two Distinct Regions of the PKA-C Substrate Binding Cleft Mediate Noncatalytic and Catalytic CFTR Stimulation.** Noncatalytic activation of CFTR by PKA-C binding must reflect stabilization of a released R domain conformation through an interaction between CFTR and PKA-C, but which region of the kinase is involved in this process is unknown. One possibility is that PKA-C uses its substrate binding site to directly "grab" a substrate loop of the R domain. Alternatively, interactions between other parts of the channel and the kinase may promote R-domain release. To differentiate between these possibilities, we studied how noncatalytic and catalytic CFTR current activation is affected by two versions of the PKA inhibitory peptide (PKI), a shorter and a longer segment of the heat-stable protein inhibitor of PKA-C (24). PKI peptides are pseudosubstrates that bind into the PKA-C substrate binding cleft (compare Fig. 1 *B Left* vs. *Right*), but in which the target serine is replaced by an alanine (Fig. 1*B*, *red*). In the 17-mer PKI(6-22)amide, the pseudosubstrate stretch (Fig. 1 *B*, *Right*, *light purple*) is preceded by an amphipathic α-helix (*dark purple*); lack of that helix in the shorter PKI(14-22) amide is reflected by its lower affinity for PKA-C ($K_I$ ~36 nM vs. ~1.7 nM (25)).

To test competitive inhibition by PKI peptides, we purified bovine PKA-C (bPKA-C) from beef heart [(26); *Materials and Methods*; *SI Appendix*, Fig. S1 *A* and *C*) and assessed block of phosphorylation by bPKA-C of the fluorescently labeled soluble peptide substrate TAMRA-kemptide (27). Kemptide phosphorylation is reported by a decrease in mobility on thin layer chromatography (TLC) sheets (23) (Fig. 1 *D–F*, *Bottom*), allowing reconstruction of phosphorylation time courses by densitometry (Fig. 1 *D–F*, *Top*). In control experiments using 5 nM bPKA-C and 20 μM TAMRA-kemptide, ~50% of the substrate (i.e., ~10 μM) was phosphorylated in <3 min (Fig. 1*D*), yielding a $k_{cat}$ estimate of ~12 $s^{-1}$ (Fig. 1*C*, *red bar*). In rough agreement with the reported $K_I$ values and the $K_M$ of TAMRA-kemptide [~2 μM (27)], application of 0.2 μM PKI(6-22)amide (Fig. 1*E*) or 10 μM PKI(14-22)amide (Fig. 1*F*) slowed phosphorylation time courses by seven- to eightfold (Fig. 1*C*, *striped bars*). (See calculation of expected fractional inhibition in *Materials and Methods*.)

Exposure of inside-out macropatches containing wild-type (WT) CFTR channels to 2 mM ATP + 300 nM bPKA-C (Fig. 1*G*, *gray* and *red bars*) causes both reversible and irreversible CFTR current activation. The irreversible component which survives bPKA-C removal (Fig. 1*G*; Fig. 1*L, gray bars*) reports the effect on channel gating of phosphorylation per se and develops over the time course of tens of seconds. Applying bPKA-C first for 1 min, and then for additional 3 min to reach full phosphorylation (Fig. 1*G*), reveals that the irreversible component reaches ~70% of its final value already after 1 min in bPKA-C (Fig. 1*L*, compare *gray bars* identified by *double arrow*), whereas the rapidly reversible component roughly doubles the open probability of phosphorylated channels (Fig. 1*L*, *red bars*). Coapplication of 5 μM PKI(6-22)amide during the first 1-min exposure to bPKA-C (Fig. 1*H*; 1st *purple bar*) abolished current activation, reporting complete inhibition of channel phosphorylation (Fig. 1*M*, compare *arrowed gray bars*). Moreover, reversible stimulation of phosphorylated channels by reapplied bPKA-C (Fig. 1*H*; 3rd *red bar*) was also entirely blocked by coapplied PKI(6-22)amide (Fig. 1*H*; 2nd *purple bar*; Fig. 1*M*, *striped* vs. *red bar*). When 20 μM PKI(14-22)amide was coapplied during the first 1-min bPKA-C exposure (Fig. 1*I*, 1st *light purple bar*) irreversible current activation was also greatly reduced, reaching only ~8% of its final value (Fig. 1*N*, compare *arrowed gray bars*). However, in stark contrast to the action of the longer PKI, the shorter peptide failed to suppress rapid reversible stimulation of phosphorylated channels by reapplied bPKA-C (Fig. 1*I*; 3rd *red bar*; Fig. 1*N*, *striped* vs. *red bar*). A systematic screening of PKI peptides with the N terminus incrementally extended from position 14 to 6 further narrowed down the region which blocks reversible CFTR activation to PKI residues 6–9 (*SI Appendix*, Fig. S2).

Pure noncatalytic activation of unphosphorylated channels by bPKA-C can be studied in the presence of 10 μM $N^6$-(2-phenylethyl)-ATP (P-ATP; Fig. 1 *J* and *K*, *dark gray bars*), an ATP analog that opens CFTR channels with high affinity but cannot be used by PKA-C for phosphotransfer (23). The strong reversible stimulation of unphosphorylated channels by bPKA-C in P-ATP was also largely prevented by 5 μM PKI(6-22)amide (Fig. 1*J*, *purple bar*; Fig. 1*O*, *striped* vs. *red bar*), whereas it was unaffected by PKI(14-22)amide even at a concentration as high as 100 μM (Fig. 1*K*, *light purple bar*; Fig. 1*P*, *striped* vs. *red bar*). Thus, the specific subregion of the PKA-C substrate cleft which accommodates the N-terminal helix (residues 6–13) of PKI(6-22)amide (Fig. 1*B*, *dark purple*) is responsible for rapid noncatalytic stimulation of both unphosphorylated and phosphorylated CFTR (Fig. 1*A*, states 3 and 4).

**PKA-C Posttranslational Modification Pattern Profoundly Affects Efficiency of CFTR Stimulation.** To facilitate structure/function studies of the CFTR/PKA-C interaction, the bovine PKA-C protein was expressed in *Escherichia coli* and affinity-purified to homogeneity (*SI Appendix*, Fig. S1 *B* and *C*). Although the amino acid sequence of this recombinant PKA-C (rPKA-C) is identical to that of native bPKA-C, their posttranslational modification patterns are different (28). We therefore first compared their catalytic activities on TAMRA-kemptide

(Fig. 2 *A* and *B*). Phosphorylation time courses for parallel preparations of rPKA-C and bPKA-C were similar, reporting $k_{cat}$ values of ~7 $s^{-1}$ and ~9 $s^{-1}$, respectively (Fig. 2*C*; $P = 0.085$).

Surprisingly, despite being fully catalytically competent on a soluble substrate, CFTR current activation by rPKA-C was greatly impaired compared to that by bPKA-C (Fig. 2*D*). In the presence

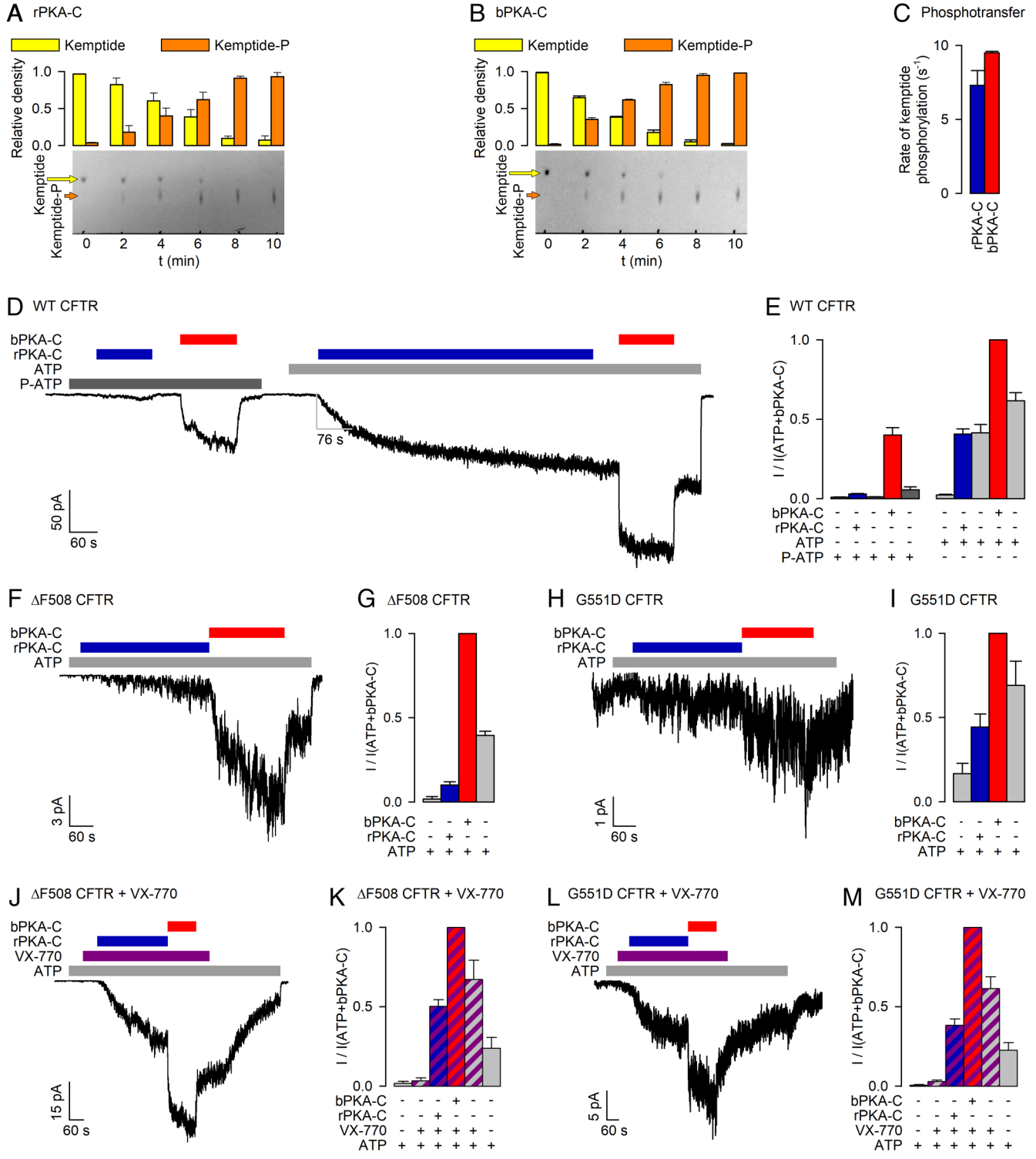


**Fig. 2.** Recombinant PKA-C is fully active on a soluble substrate, but poorly activates CFTR. (*A* and *B*) Time courses of kemptide phosphorylation resolved on TLC sheets (*Bottom*) and densitometric analysis (*Top*) for rPKA-C (*A*) or bPKA-C (*B*). Conditions and color coding as in Fig. 1 *D–F*. (*C*) Calculated $k_{cat}$ ($s^{-1}$) for rPKA-C (*blue*) and bPKA-C (*red*). Data in *A–C* represent mean ± SEM, n = 3. (*D*) Macroscopic WT CFTR current activated by repeated exposures to 300 nM rPKA-C (*blue bars*) or bPKA-C (*red bars*) in the presence of either 10 μM P-ATP (*dark gray bar*) or 2 mM ATP (*light gray bar*). (*E*) Steady-state currents in the sequential segments of the experiment in *D*, normalized to that in the presence of ATP+bPKA-C (*2nd red column*). Data represent mean ± SEM, n = 5 to 6. (*F*) Macroscopic current from ΔF508 CFTR channels activated by 300 nM rPKA-C (*blue bar*) or bPKA-C (*red bar*) in 2 mM ATP (*gray bar*). (*G*) Steady-state currents in the sequential segments of the experiment in panel *F*, normalized to that in the presence of ATP+bPKA-C. (*H* and *I*) Data analogous to those in panels *F* and *G*, but for G551D CFTR channels. (*J*) Macroscopic current from ΔF508 CFTR channels activated by 300 nM rPKA-C (*blue bar*) or bPKA-C (*red bar*) in 2 mM ATP (*gray bar*), in the presence of 10 nM VX-770 (*purple bar*). (*K*) Steady-state currents in the sequential segments of the experiment in panel *J*, normalized to that in the presence of ATP+bPKA-C + VX-770. (*L* and *M*) Data analogous to those in panels *J* and *K*, but for G551D CFTR channels. Data in *G*, *I*, *K*, and *M* represent mean ± SEM, n = 4 to 6.

of P-ATP, 300 nM rPKA-C failed to reversibly activate unphosphorylated CFTR (Fig. 2 *D* and *E*, *left*, *blue bars*). In the presence of ATP (Fig. 2 *D*, *Right*), CFTR current activation by rPKA-C was greatly slowed compared to that by bPKA-C (cf., Fig. 1*G*), and the maximal current achieved after ~5 min was less than half of that evoked by subsequent exposure to 300 nM bPKA-C (Fig. 2 *D* and *E*, *Right*, *blue* vs. *red bar*). That smaller maximal current was in part due to a complete lack of reversible stimulation of phosphorylated channels by rPKA-C, as evidenced by a lack of current decline following its removal (Fig. 2 *E*, *Right*, *2nd* vs. *3rd bar*). In addition, the steady current that survived rPKA-C removal was significantly ($P = 0.012$) smaller than the current following a subsequent exposure to bPKA-C (Fig. 2 *E*, *Right*, *3rd* vs. *5th bar*), suggesting that CFTR channels are phosphorylated by rPKA-C not only far slower but also to a somewhat lower final stoichiometry. Similar results were obtained when comparing PKA-C proteins from various commercial sources: whereas native preparations [Sigma-Aldrich P2645 (23) and 539576 (*SI Appendix*, Fig. S3 *A* and *C*)] functionally resembled our bPKA-C, recombinant products (Promega V5161) recapitulated our findings on rPKA-C (*SI Appendix*, Fig. S3 *B* and *C*). These results suggest that the CFTR/PKA-C interaction is highly sensitive to some posttranslational modification of PKA-C.

Because PKA-C posttranslational modification patterns might dynamically change in vivo, differential efficacies of different PKA-C isoforms might bear relevance to CF disease. We therefore compared the efficacies of rPKA-C and bPKA-C for activation of CFTR channels bearing the ΔF508 or G551D mutation. Interestingly, rPKA-C was even less efficient in activating currents for the disease mutants. Compared to bPKA-C, maximal current activated by rPKA-C was only ~10% and 40%, respectively, for ΔF508 and G551D CFTR (Fig. 2 *F* and *H*; Fig. 2 *G* and *I*, *blue* vs. *red bars*).

An increasing number of CF patients worldwide receive treatment with the potentiator VX-770, administered alone or in combination with corrector drugs. As CFTR gating stimulation by VX-770 requires prior phosphorylation of CFTR (7), and rPKA-C might fail to fully phosphorylate mutant CFTR channels (Fig. 2 *F*–*I*), we compared the efficacies of rPKA-C and bPKA-C for channel activation in the presence of the drug (Fig. 2 *J* and *L*). As expected, unphosphorylated channels were only marginally stimulated by 10 nM VX-770 (Fig. 2 *K* and *M*; *2nd bar*), a quasi-saturating concentration of the drug [$EC_{50}$~1.5 nM, (29)]. In addition, even in the presence of the drug, for both mutants, steady-state activation by rPKA-C was substantially reduced compared to that by bPKA-C (Fig. 2 *K* and *M*, compare *3rd* and *4th bars*).

**Enzymatic Demyristoylation of Bovine PKA-C Diminishes Noncatalytic and Catalytic CFTR Activation.** One documented structural difference between the two PKA-C isoforms is that native bPKA-C is N-myristoylated (16), whereas rPKA-C is not (30). To address whether the PKA-C N-myristoyl group is essential for a fruitful CFTR/PKA-C interaction, we took advantage of the Invasion plasmid antigen J (IpaJ) protein, a cysteine-protease injected by *Shigella flexneri* into the cytosol of infected cells. When expressed in vitro, the IpaJ catalytic core domain (residues 51–259) nonspecifically demyristoylates a large number of proteins, including PKA-C, by cleaving the peptide bond following the N-myristoylated glycine (31). The IpaJ catalytic domain was expressed in *E. coli* and affinity-purified (*SI Appendix*, Fig. S4 *A* and *B*). To test its activity, a fluorescently labeled synthetic peptide encompassing the first 11 residues of PKA-C was synthesized in both N-myristoylated ("myr-peptide") and nonmyristoylated ("nonmyr-peptide") forms. The higher mobility of the myr-peptide on TLC sheets (Fig. 3*A*, *lanes 1* and *2*) allows to monitor its demyristoylation. Indeed, a 10-min incubation of 50 μM myr-peptide with 3 μM IpaJ at room temperature completely converted the myr-peptide into a low-mobility product, consistent with cleavage of the N-terminal myr-glycine group (Fig. 3*A*, *lane 3*).

To test the effect of IpaJ treatment on full-length bPKA-C, the kinase was purified from beef heart, tested for catalytic activity on kemptide (Fig. 3*B*; Fig. 3*D*, *red bar*), and then incubated with IpaJ (molar ratio 5:1) at 37 °C for 3 h. IpaJ was then selectively removed and bPKA-C concentration redetermined (*Materials and Methods*; *SI Appendix*, Fig. S4*C*). IpaJ treatment did not affect the catalytic activity of bPKA-C toward soluble kemptide (Fig. 3*C*; Fig. 3*D*, *light blue bar*). However, WT CFTR channels prephosphorylated by a 3-min exposure to 300 nM untreated bPKA-C (Fig. 3*E*, *red bar*) failed to respond to subsequent application of 300 nM IpaJ-treated bPKA-C (Fig. 3*E*, *light blue bar*), revealing complete lack of noncatalytic stimulation of phosphorylated CFTR (Fig. 3*F*, *red* vs. *light blue bar*). Exposure of unphosphorylated WT CFTR channels to 300 nM IpaJ-treated bPKA-C resulted in slower current activation compared to untreated bPKA-C (cf., Fig. 3 *E* and *G*), reporting a slowed rate of CFTR phosphorylation, and failed to maximally activate channel currents (Fig. 3 *G* and *H*, *first blue* vs. *red bar*). To quantitatively compare rates of CFTR current activation by PKA-C variants applied at 300 nM, the time required for half-maximal current activation ($t_{1/2}$; cf., *gray L-bars* in Figs. 2*D* and 3 *E* and *G*) was normalized to $t_{1/2}$ for activation by bPKA-C measured in the same batches of cells. Just as for rPKA-C (Fig. 3*I*, *dark blue bar*), $t_{1/2}$ for IpaJ-treated bPKA-C was ~4-fold longer compared to untreated bPKA-C (Fig. 3*I*, *red* vs. *light blue bar*). Thus, IpaJ-treated bPKA-C activates CFTR channels as inefficiently as rPKA-C.

**Coexpression of N-Myristoyl Transferase with Recombinant PKA-C Partially Restores Efficiency of CFTR Activation.** N-myristoyl transferase (NMT) is not endogenously present in *E. coli*, but recombinant PKA-C can be myristoylated either by coexpression of NMT with PKA-C in the bacteria (32), or by in vitro coincubation of purified rPKA-C and NMT proteins with myristoyl-CoA (33). In vitro incubation of 100 μM nonmyr-peptide with 17 μM purified NMT protein + 100 μM myr-CoA indeed resulted in the appearance of the myr-peptide spot (Fig. 4*A*, lane 3) which could be readily reconverted into the slowly migrating form by subsequent treatment with IpaJ (Fig. 4*A*, lane 4). However, in vitro myristoylation remained incomplete (fractional myristoylation failed to reach 100% even following overnight incubation; Fig. 4*A*, lane 3), and attempts to in vitro myristoylate rPKA-C resulted in protein aggregation.

To overcome this limitation, PKA-C was coexpressed with NMT in *E. coli*, and rPKA-C was affinity purified (*SI Appendix*, Fig. S1 *B* and *C*). Phosphotransfer activities of the resulting enzyme ("rPKA-C/NMT") and of a control preparation of rPKA-C toward kemptide (Fig. 4 *B* and *C*) were similar (Fig. 4 *F*, *Left*). However, a comparison of CFTR current activation kinetics (Fig. 4*G*) by 300 nM bPKA-C (*red trace*), rPKA-C (*blue trace*), or rPKA-C/NMT (*brown trace*), studied in the same batch of CFTR-expressing cells, revealed a clearly intermediate phenotype for rPKA-C/NMT. Whereas $t_{1/2}$ for CFTR activation was ~6-fold longer for rPKA-C compared to bPKA-C (Fig. 4 *J*, *Left*, *blue* vs. *red bar*), for rPKA-C/NMT $t_{1/2}$ was only ~2-fold longer (Fig. 4 *J*, *Left*, *brown* vs. *red bar*). Consistent with earlier reports (34), these results suggest that NMT coexpression yields partially myristoylated rPKA-C. Based on the effect of NMT coexpression on $t_{1/2}$, the estimated myristoylation efficiency is 20 to 30% (*Materials and Methods*), too low to restore reversible CFTR activation: although in some patches, a small current reduction following

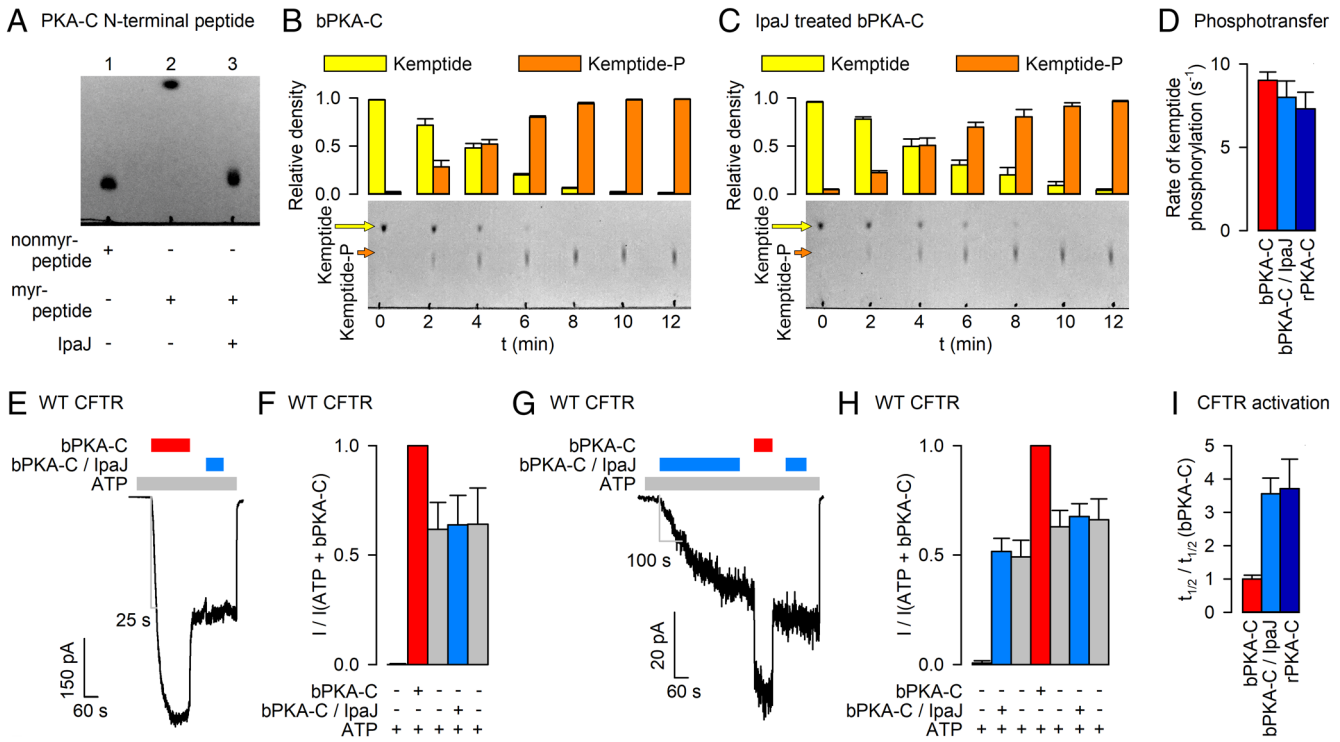


**Fig. 3.** Enzymatic demyristoylation of bPKA-C selectively impairs efficiency toward CFTR. (*A*) TLC sheet showing demyristoylation of synthetic PKA-C N-terminal peptide by purified IpaJ. Nonmyr-peptide, GNAAAAKKGSE-K-ε-TAMRA (*lane 1*); myr-peptide, N-myristoyl-GNAAAAKKGSE-K-ε-TAMRA (*lane 2*); 50 μM myr-peptide was incubated with 3 μM IpaJ for 10 min at room temperature (*lane 3*). (*B* and *C*) Time courses of kemptide phosphorylation resolved on TLC sheets (*Bottom*) and densitometric analysis (*Top*) for control bPKA-C (*B*) or IpaJ-treated (*Materials and Methods*) bPKA-C (*C*). Conditions and color coding as in Fig. 1 *D–F*. (*D*) Calculated $k_{cat}$ ($s^{-1}$) for bPKA-C (*red*), IpaJ-treated bPKA-C (*light blue*), and rPKA-C (*dark blue*; replotted from Fig. 2*C*). Data in *B–D* represent mean ± SEM, n = 3. (*E*) WT CFTR current initially activated by 300 nM bPKA-C (*red bar*) and then exposed to 300 nM IpaJ-treated bPKA-C (*light blue bar*). (*F*) Steady-state currents in the sequential segments of the experiment in panel *E*, normalized to that in the presence of ATP+bPKA-C (*red bar*). Data represent mean ± SEM, n = 7. (*G*) WT CFTR current initially activated by 300 nM IpaJ-treated bPKA-C (*light blue bar*) and then exposed to 300 nM bPKA-C (*red bar*). (*H*) Steady-state currents in the sequential segments of the experiment in panel *G*, normalized to that in the presence of ATP+bPKA-C (*red bar*). Data represent mean ± SEM, n = 5. (*I*) Time required for half-maximal CFTR current activation ($t_{1/2}$; cf., gray L-bars in Figs. 2*D*, and 3 *E* and *G*) for IpaJ-treated bPKA-C (*light blue bar*) and rPKA-C (*dark blue bar*), normalized to $t_{1/2}$ for activation by bPKA-C obtained in patches from the same batches of oocytes (*red bar*). Data represent mean ± SEM, n = 5 to 10.

rPKA-C/NMT removal could be observed, the effect proved insignificant (Fig. 4*I*, *brown bar*) [cf., (23)]. However, when studied on the background of the tiny currents of nonphosphorylated channels gating in P-ATP, a condition that greatly amplifies the fractional effect of noncatalytic activation (cf., Fig. 1 *J* and *K*; Fig. 1 *O* and *P*, *red* vs. *gray bars*), reversible current stimulation by rPKA-C/NMT was significantly enhanced ($P = 0.0009$) compared to that by rPKA-C (*SI Appendix*, Fig. S5 *A* and *B*, *brown* vs. *blue bars*), reaching ~25% of that by bPKA-C (*SI Appendix*, Fig. S5 *A* and *B*, *brown* vs. *red bars*).

**Phosphorylation at Serine 10 of PKA-C Does Not Affect Its Efficiency to Activate CFTR.** A second distinguishing structural feature of rPKA-C is its reported autophosphorylation at serine 10 (28). Indeed, LC–MS/MS analysis of our PKA-C preparations confirmed that bPKA-C is not phosphorylated at this position, whereas rPKA-C is phosphorylated to a stoichiometry of ~40% [five versus eight recovered peptide fragments (*SI Appendix*, Fig. S6)]. To address the impact of that difference on CFTR channel activation, PKA-C bearing the S10A mutation was expressed in *E. coli* with or without NMT. As reported previously (35), the majority of the mutant PKA-C was targeted to inclusion bodies, reporting a negative effect of the S10A mutation on folding efficiency. Nevertheless, for both S10A rPKA-C and S10A rPKA-C/NMT sufficient amounts could be purified from the soluble fractions (*SI Appendix*, Fig. S1 *B* and *C*) to allow functional analysis. Both mutant proteins were active when assayed on kemptide (Fig. 4 *D* and *E*), but showed a modest reduction in phosphotransfer rates (Fig. 4*F*, cf., *checkered* vs. *noncheckered bars*) which was significant for S10A rPKA-C (~2-fold, $P = 0.0005$). However, CFTR channel activation by S10A rPKA-C (Fig. 4*H*, *blue trace*) resembled that by WT rPKA-C: $t_{1/2}$ for current activation was ~5-fold prolonged compared to bPKA-C (Fig. 4*J*, *blue checkered bar*), and reversible stimulation was undetectable (Fig. 4*I*, *blue checkered bar*). Importantly, just as for WT rPKA-C, NMT coexpression increased the efficiency of CFTR current activation by S10A rPKA-C (Fig. 4*H*, *brown trace*): $t_{1/2}$ was shortened (Fig. 4*J*, *brown checkered bar*), and even a small (~1.25-fold) but significant ($P = 0.003$) reversible stimulation was restored (Fig. 4*I*, *brown checkered bar*).

**Uncharacterized IpaJ Homologs Are Present in the Genomes of Gram-Negative CF Pathogens.** *Pseudomonas*, *Burkholderia*, and *Stenotrophomonas* genera are among the most common CF pathogens, and all three contain secretion systems that deliver effector proteins into the host cell cytosol (36). However, to date, only a small subset of these secreted virulence factors have been identified. The *Shigella* effector protein IpaJ is a member of the cysteine peptidase C39-like family which includes many uncharacterized members in more than 200 bacterial species (31, 37). Using a BLAST search we identified several IpaJ homologs also in the three most CF-relevant bacterial genera (Fig. 5*A*).

To test whether enzymes capable of removing N-myristoyl glycines from target proteins may be present also in these bacteria, we expressed and purified (*SI Appendix*, Fig. S4 *A* and *B*) the catalytic domain of the *Pseudomonas* sequence with highest homology to IpaJ (WP_150780237.1; Fig. 5*A*, *blue frame*). When tested on the

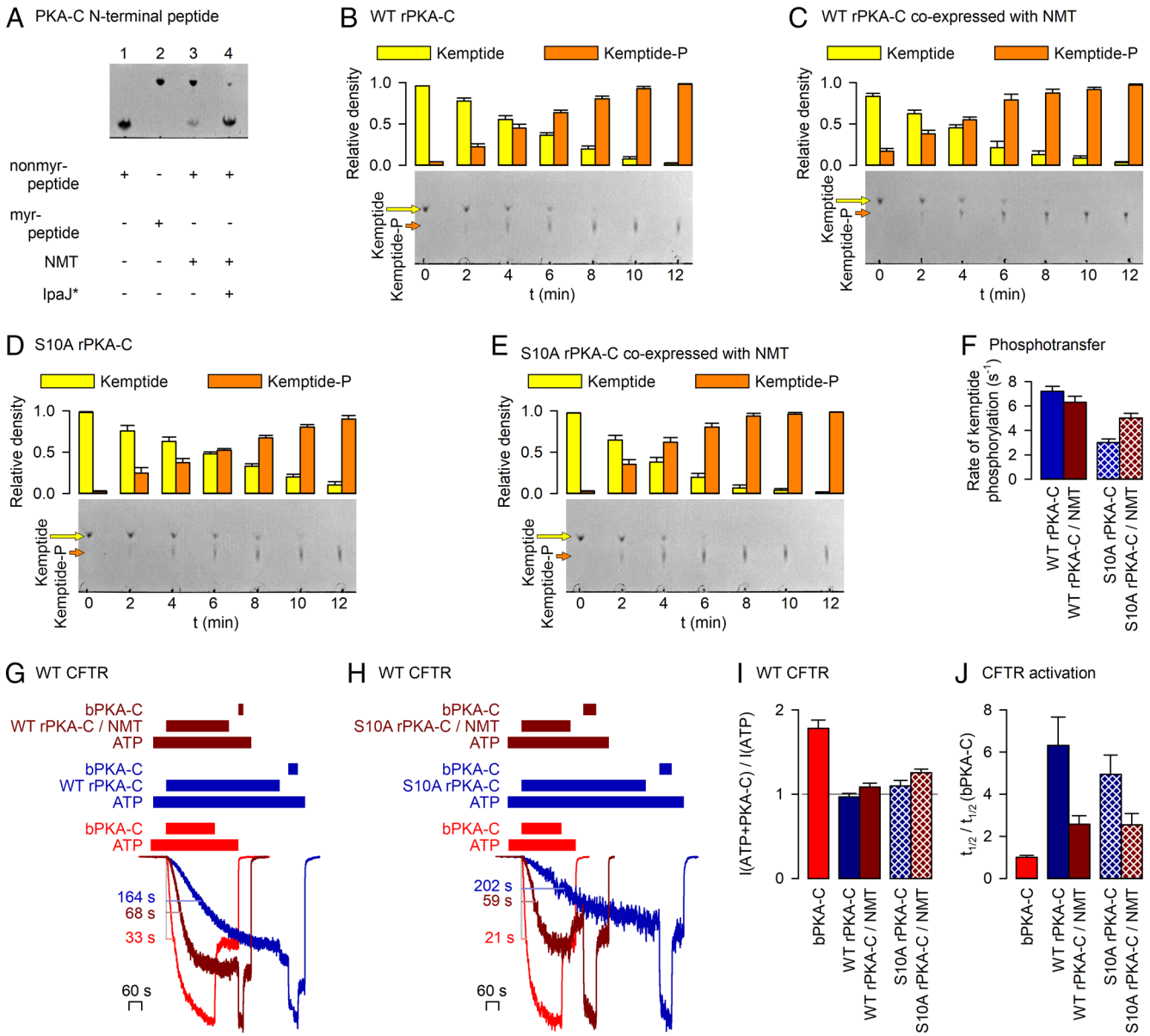


**Fig. 4.** NMT coexpression partially restores rPKA-C efficiency toward CFTR. (*A*) TLC sheet showing in vitro myristoylation of synthetic PKA-C N-terminal peptide by purified NMT. Controls, nonmyr-peptide (*lane 1*) and myr-peptide (*lane 2*); 100 μM nonmyr-peptide was incubated with 17 μM NMT + 100 μM myr-CoA overnight at room temperature (*lane 3*). *An aliquot of the reaction product was subsequently treated with 3 μM IpaJ for 10 min (*lane 4*). (*B–E*) Time courses of kemptide phosphorylation resolved on TLC sheets (*Bottom*) and densitometric analysis (*Top*) for control rPKA-C (*B*), rPKA-C coexpressed with NMT (*C*), control S10A rPKA-C (*D*), or S10A rPKA-C coexpressed with NMT (*E*). 5 nM rPKA-C (*B*), 8 nM rPKA-C/NMT (*C*), 10 nM S10A rPKA-C (*D*), or 10 nM S10A rPKA-C/NMT (*E*) was incubated with 20 μM TAMRA-kemptide + 200 μM MgATP for the indicated amounts of time at room temperature. Color coding as in Fig. 1 *D–F*. (*F*) Calculated $k_{cat}$ ($s^{-1}$) for control rPKA-C (*dark blue*), rPKA-C/NMT (*brown*), control S10A rPKA-C (*dark blue checkered*), and S10A rPKA-C/NMT (*brown checkered*). Data in *B–F* represent mean ± SEM, n = 3. (*G* and *H*) Overlays of three WT CFTR current traces, activated by 300 nM of (*G*) bPKA-C (*red trace*), rPKA-C (*dark blue trace*), or rPKA-C/NMT (*brown trace*) and (*H*) bPKA-C (*red trace*), S10A rPKA-C (*dark blue trace*), or S10A rPKA-C/NMT (*brown trace*), respectively. For the *dark blue* and *brown traces*, 300 nM bPKA-C was subsequently applied. Currents were synchronized to the time point of the first PKA-C application and normalized to the steady-state amplitude in 300 nM bPKA-C. Color coding of bars that identify exposure to compounds follows that of the respective current traces. (*I*) Noncatalytic stimulation by bPKA-C (*red*), rPKA-C (*dark blue*), rPKA-C/NMT (*brown*), S10A rPKA-C (*dark blue checkered*), and S10A rPKA-C/NMT (*brown checkered*), expressed as the ratio of mean steady current in ATP+PKA-C to that following PKA-C removal. (*J*) Time required for half-maximal CFTR current activation ($t_{1/2}$; cf., colored L-bars in panels *G* and *H*) by PKA-C variants, normalized to $t_{1/2}$ for activation by bPKA-C obtained in patches from the respective batches of oocytes. Color coding as in panel *I*. Data in *I* and *J* represent mean ± SEM, n = 6 to 12.

PKA-C N-terminal myr-peptide, this "PsIpaJ" protein also readily removed the N-myristoyl glycine (Fig. 5*B*). Moreover, treatment of bPKA-C with PsIpaJ (*SI Appendix*, Fig. S4*D*) resulted in functional effects similar to those of IpaJ treatment. Compared to untreated bPKA-C, CFTR current activation by PsIpaJ-treated bPKA-C was ~3-fold slower (Fig. 5*E*; Fig. 5*G*, *light blue bar*), and reversible CFTR activation was largely diminished, as reported by a virtual lack of current decline upon its removal (Fig. 5 *E* and *F*, *blue* vs. subsequent *gray bars*). On the other hand, the $k_{cat}$ for kemptide phosphorylation was unaffected by PsIpaJ treatment (Fig. 5 *C* and *D*).

## Discussion

The molecular mechanisms by which PKA-C activates CFTR have only started to become clear (Fig. 1*A*). Here, we show that non-catalytic CFTR activation requires a specific small region near to, but distinct from the PKA-C substrate binding site: whereas, as

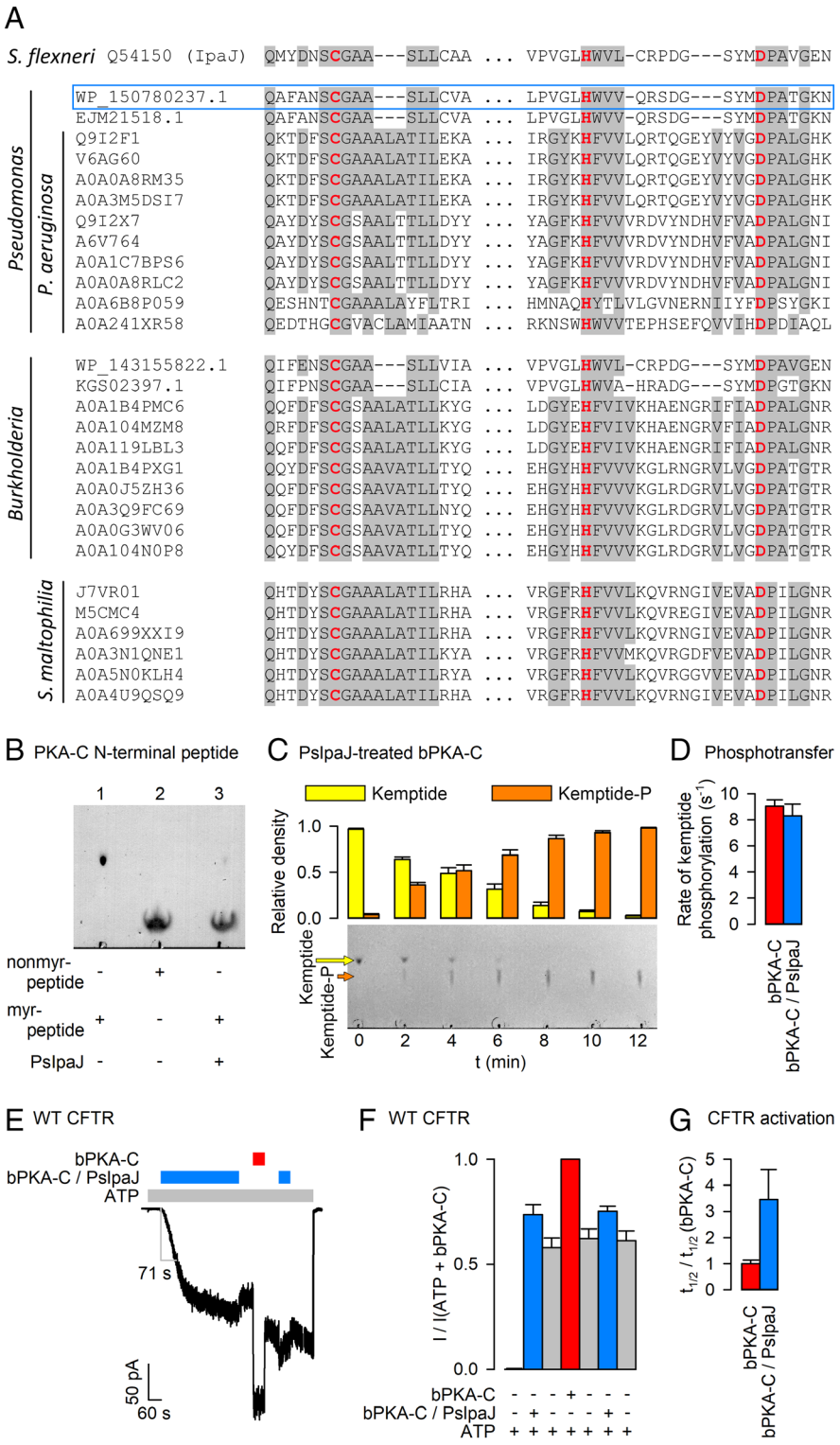


**Fig. 5.** *Pseudomonas* IpaJ homolog demyristoylates bPKA-C in vitro. (*A*) Sequence alignment of catalytically important segments of *S. flexneri* IpaJ with homologous sequences identified in the genomes of *Pseudomonas* (*Top* block), *Burkholderia* (*Center* block), and *Stenotrophomonas* (*Bottom* block) genera. *Gray*, conserved residues; *bold red*, cysteine protease catalytic triad; *blue box*, *Pseudomonas* sequence most closely related to IpaJ (PsIpaJ). (*B*) TLC sheet showing demyristoylation of synthetic PKA-C N-terminal peptide by purified PsIpaJ. Myr-peptide, N-myristoyl-GNAAAAKKGSE-K-ε-TAMRA (*lane 1*); nonmyr-peptide, GNAAAAKKGSE-K-ε-TAMRA (*lane 2*); 30 μM myr-peptide was incubated with 0.5 μM PsIpaJ for 30 min at room temperature (*lane 3*). (*C*) Time course of kemptide phosphorylation resolved on TLC sheet (*Bottom*) and densitometric analysis (*Top*) for PsIpaJ-treated (*Materials and Methods*) bPKA-C. Conditions and color coding as in Fig. 1 *D*–*F*. (*D*) Calculated $k_{cat}$ ($s^{-1}$) for bPKA-C (*red*; replotted from Fig. 3*D*) and PsIpaJ-treated bPKA-C (*light blue*) from the densitometric analysis in *C*. Data represent mean ± SEM, n = 3. (*E*) WT CFTR current initially activated by 300 nM PsIpaJ-treated bPKA-C (*light blue bar*) and then exposed to 300 nM untreated bPKA-C (*red bar*). (*F*) Steady-state currents in the sequential segments of the experiment in *E*, normalized to that in the presence of ATP+bPKA−C (*red bar*). (*G*) Time required for half-maximal CFTR current activation ($t_{1/2}$; cf., gray L-bar in panel *E*) for PsIpaJ-treated bPKA-C (*light blue bar*), normalized to $t_{1/2}$ for activation by bPKA-C obtained in patches from the same batches of oocytes (*red bar*). Data in panels *F* and *G* represent mean ± SEM, n = 8 to 9.

expected, catalytic CFTR stimulation (i.e., phosphorylation) is prevented by both short and long PKI pseudosubstrate peptides (Fig. 1 *H*, *I*, *M*, and *N*, *arrowed gray bars*), noncatalytic activation of both unphosphorylated and phosphorylated CFTR channels is specifically blocked by the short amphipathic helix (Fig. 1*B*, right, *dark purple*) formed by residues 6–13 of PKI(6-22)amide (Fig. 1 *H* and *I*, Fig. 1 *M* and *N*, *striped bars*). Comparison of $K_I$ values of the short and long peptide suggests a low (millimolar) affinity for binding of the N-terminal helix per se to PKA-C. (See estimation of $K_I$ values in *Materials and Methods*.) Nevertheless, at a concentration of 1 mM, near its solubility limit, PKI(6-13)amide did not significantly affect catalytic CFTR activation ($P = 0.08$) but significantly ($P = 6 \times 10^{-6}$) suppressed noncatalytic activation of phosphorylated channels by 300 nM bPKA-C (*SI Appendix*, Fig. S7).

One interpretation is that the small hydrophobic patch on the PKA-C surface which accommodates PKI(6-13)amide serves as a "docking site" (Fig. 6, *Top Left*, "d"): binding of an R-domain segment adjacent to a target serine loop would help to present the latter for catalysis (Fig. 6, *Top Left*, *asterisk* marks binding site of

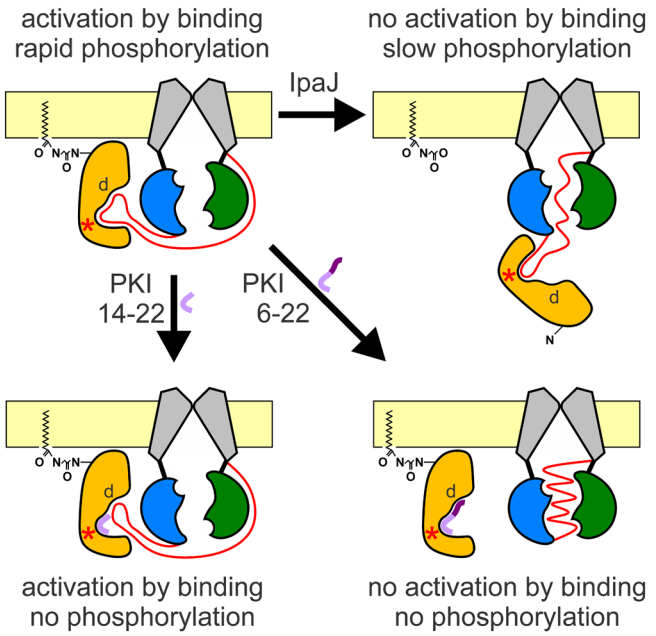


**Fig. 6.** Structural requirements for efficient CFTR/PKA-C interaction. Cartoon color coding as in Fig. 1*A*. (*Top Left*) Membrane-tethering of PKA-C properly orients its catalytic cleft for binding substrate segments of the CFTR R domain, causing both noncatalytic activation and rapid phosphorylation of CFTR. *Red asterisk*, binding site for target serine, d, docking site. (*Top Right*) Cysteine protease-mediated cleavage of the N-myristoyl-glycine from PKA-C untethers the enzyme from the membrane, preventing noncatalytic activation and slowing phosphorylation of CFTR. (*Bottom Left*) Pseudosubstrate peptide PKI(14-22)amide (light *violet ribbon*) blocks the active site but leaves the docking site accessible for R-domain binding, preventing phosphorylation but not noncatalytic activation. (*Bottom Right*) Pseudosubstrate peptide PKI(6-22)amide (*violet ribbon*; *light segment*, substrate loop; *dark segment*, amphipathic helix) blocks PKA-C/R-domain interaction, preventing both noncatalytic activation and phosphorylation.

target serine). That mechanism would explain why noncatalytic stimulation is preserved even in phosphorylated channels (Fig. 1*L*, *right red bar*), even though phosphorylation dramatically decreases the binding affinity of target serine loops for the kinase (38). By blocking the entire substrate binding cleft, including both the active site and the docking site, the long peptide PKI(6-22)amide would prevent R-domain docking and thereby even noncatalytic stimulation (Fig. 6, *Bottom Right*). In contrast, the shorter PKI(14-22)amide leaves the docking site unoccupied allowing R-domain docking and noncatalytic stimulation (Fig. 6, *Bottom Left*). Interestingly, noncatalytic stimulation of phosphorylated channels was even slightly (but significantly, $P = 0.02$) enhanced by the presence of PKI(14-22)amide (Fig. 1*I*; Fig. 1*N*, *red* vs. *subsequent striped bar*; cf. *SI Appendix*, Fig. S2). Because binding of long PKI peptides induces closure of the substrate cleft (39–41) we speculate that PKI(14-22) binding may also induce some degree of cleft closure which slightly enhances the binding affinity of the docking site for R-domain loops. However, that affinity might still be quite low, considering the small PKA-C surface area involved and its low affinity for PKI(6-13)amide (*SI Appendix*, Fig. S7). Correspondingly, sequence comparison between the R domain and PKI(6-13) (*SI Appendix*, Fig. S8) did not reveal any homologous stretches. Moreover, the binding sites of other PKA-C substrates for which structures in complex with the kinase are available, such as the PKA-R subunit (42), the type 2 Ryanodine Receptor (43), or phospholamban (44), are distinct from the docking site identified here, excluding their usefulness for a targeted sequence search. Importantly, it must be emphasized that the docking site model is just one possible interpretation of our observations. An alternative possibility would be that interaction of that hydrophobic patch on PKA-C (Fig. 6, "d") with some other part of CFTR is required for promoting R domain release from its wedged-in position.

We also show here that phosphotransfer by PKA-C is not the rate-limiting step for catalytic CFTR activation. If that were the case, with a $k_{cat}$ of ~10 $s^{-1}$ (Figs. 1*C*, 2*C*, and 3*D*, *red*), all ~10 target serines in the R domain should be phosphorylated within ~1 s. Indeed, although that $k_{cat}$ was determined using kemptide as a substrate here (Fig. 1 *C* and *D*), similar values were found earlier using short synthetic peptides encompassing the regions around 7 of the 8 target serines in the R domain (45) located within dibasic PKA-C consensus motifs (46, 47) (cf., *SI Appendix*, Fig. S8, *yellow highlight*). In contrast, full activation of the irreversible component of the CFTR current requires >1 min using bPKA-C (Fig. 1 *G* and *L*, *gray bars*), and >5 min using rPKA-C (Figs. 2*D* and 4*G*, *blue trace*). Correspondingly, the modest reduction in phosphotransfer rate of S10A rPKA-C (Fig. 4*F*, *blue checkered* vs. *uncheckered bar*) does not slow CFTR current activation relative to that by WT rPKA-C (Fig. 4*J*, *blue checkered* vs. *uncheckered bar*). Thus, other kinetic steps, likely related to spontaneous release of the unphosphorylated R domain from its wedged-in position (Fig. 1*A*, step 1→2), and/or targeting of PKA-C to its unstructured substrate, rate limit catalytic CFTR activation.

Along those lines, we identify here that the presence of an N-terminal myristoyl group on PKA-C fundamentally determines its efficiency toward CFTR. Whereas both myristoylated (bPKA-C) and nonmyristoylated (rPKA-C) PKA-C are equally effective on a soluble substrate (Figs. 2 *A–C* and 3 *B–D*), nonmyristoylated PKA-C only poorly activates CFTR. In particular, 300 nM nonmyristoylated PKA-C supports no noncatalytic activation (Fig. 2 *D* and *E*) and ~4- to 6-fold slower catalytic activation compared to 300 nM myristoylated PKA-C (Figs. 3*I* and 4*J*, *blue*). Moreover, even at steady state, full phosphorylation is not reached within the entire time course of our experiments (Fig. 2 *D* and *E*), suggesting that some R-domain serines might not become phosphorylated. That inefficiency of nonmyristoylated PKA-C is even more pronounced toward disease mutants ΔF508 and G551D for which maximal current in rPKA-C is only ~10% and ~40%, respectively, of that in bPKA-C (Fig. 2 *F–I*).

In support of this crucial role of the PKA-C N-myristoyl group, its enzymatic removal from the native enzyme diminishes (Fig. 3 *E–I*), whereas its incorporation into the recombinant enzyme enhances (Fig. 4 *G–J*), efficiency toward CFTR. In contrast, neither of these manipulations affects phosphotransfer activity toward a soluble substrate (Figs. 3 *B–D* and 4 *B–F*). The alternative explanation that the presence of phosphoserine 10 in rPKA-C impairs its efficiency toward CFTR is ruled out by the lack of effect of the S10A mutation on CFTR activation time courses (Fig. 4 *G* and *H*, *blue traces*; Fig. 4*J*, *blue checkered* vs. *noncheckered bars*).

Coexpression of NMT with PKA-C in *E. coli* did not result in fully myristoylated rPKA-C (Fig. 4 *G–J*). One possible reason for that inefficiency is the reported autophosphorylation of S10 in rPKA-C (28), which impedes N-myristoylation (34). However, although NMT coexpression restored a significant fraction of noncatalytic stimulation for phosphorylated S10A (but not WT) rPKA-C (Fig. 4*I*), its limited amplitude suggests that myristoylation stoichiometry remained incomplete even for the mutant. Thus, other factors, perhaps the availability of myristoyl-CoA in the bacteria, must be limiting.

The presence of an N-myristoyl group on PKA-C was discovered decades ago (16), but its exact biophysical role is still not entirely clear. Although N-myristoylated, PKA-C is a soluble cytosolic protein (48),

and the N-myristoyl group is not required for its association with the regulatory subunit, cAMP-dependent activation, phosphotransfer activity toward most substrates, or access to the nucleus (49, 50). The Type II holoenzyme is targeted to membranes, but this is thought to be primarily achieved through binding of the Type II regulatory subunit (RII) to membrane-associated A Kinase Anchoring Proteins [AKAPs (51)]. More recent work revealed that a rapid equilibrium of the PKA-C N-myristoyl group between solvent-exposed (myr-out) and protein-occluded (myr-in) conformations (52) is shifted toward myr-out by interaction with membranes (33) or with RII-type regulatory subunits (53). Moreover, the PKA-C N-myristoyl group allows AKAP-independent membrane anchoring of Type II holoenzymes (54) and also of free PKA-C subunits (55). Indeed, in intact cells, stimulation of the cAMP pathway resulted in membrane accumulation of predominantly free PKA-C subunits, allowing preferential phosphorylation of membrane substrates (55). The present study on CFTR identifies a membrane substrate which can efficiently interact exclusively with myristoylated PKA-C. That specificity is likely based on both proximity and orientation effects. Membrane accumulation increases the local concentration of myristoylated PKA-C near the CFTR channel, and physical attachment to the membrane restrains PKA-C in an optimal orientation, required for engaging the CFTR R domain (Fig. 6, *Top Left*). Severing the membrane tether from PKA-C eliminates noncatalytic stimulation and impairs R-domain phosphorylation (Fig. 6, *Top Right*).

Beyond their biophysical implications, these findings might bear relevance for human disease. Until recently, the presence of an N-myristoyl group was considered a permanent feature of a subset of proteins, but this view was changed by the identification of the *Shigella* virulence factor IpaJ, an enzyme shown to catalyze the removal of N-myristoyl groups from proteins. A major challenge in CF patient care is the treatment of recurrent lung infections, accompanied by exacerbation of pulmonary function. Such infections are most often caused by *Pseudomonas*, *Burkholderia*, and *Stenotrophomonas* species that eventually colonize the CF lung (36). Depending on the stage of the infection, these strains employ Type III, IV, and/or VI secretion systems (36, 56), or outer membrane vesicles (57, 58) to directly deliver virulence factors into the cytosol of infected cells, with or without close contact to them. However, very few of these effector proteins have been studied to date. Here, we identify in their genomes a large number of uncharacterized cysteine-protease sequences homologous to IpaJ (Fig. 5*A*), and show for one *Pseudomonas* protein that it readily demyristoylates PKA-C in vitro (Fig. 5 *B* and *E–G*). Because nonmyristoylated PKA-C activates mutant CFTR channels even less efficiently (Fig. 2 *F–I*), also in the presence of a potentiator (Fig. 2 *J–M*), PKA-C demyristoylation in lung epithelial cells might further impair residual CFTR function in infected CF patients. Of note, although IpaJ also demyristoylates a broad range of target proteins in vitro (31), in host cell infection models its substrate specificity was narrow, suggesting an unknown regulatory mechanism (37). Thus, among the large number of IpaJ homologs in CF pathogens, it will be interesting to search for enzymes that target PKA-C also in vivo. Identification of such effector proteins might define novel drug targets for the treatment of CF lung disease.

## Materials and Methods

See *SI Appendix, SI Materials and Methods* for a more detailed description of experimental protocols and analyses.

***X. laevis* Oocyte Isolation and Injection.** *X. laevis* oocytes were isolated and injected with cRNA as described (59). Current recordings were obtained 1 to 3 d after injection.

**Molecular Biology.** The coding sequences of bovine protein kinase A catalytic subunit alpha and of the catalytic domains of IpaJ and PsIpaJ, with C-terminal Twin-Strep-tags, were incorporated into pJ411. NMT from *Cryptosporidium parvum* Iowa II with C-terminal $His_6$-tag was subcloned into pET14b. The cDNA for WT and mutant CFTR in pGEMHE was transcribed in vitro, and purified cRNA was stored at −80 °C.

**Protein Purification.** The catalytic subunit of protein kinase A was purified from beef heart as described (26). The obtained bPKA-C was stored at 4 °C and was stable for several months without appreciable loss of catalytic activity or efficiency toward CFTR. Recombinant bovine PKA-C was purified from *E. coli* BL21(DE3) transformed with pJ411-PKA-C. Following induction with 0.1 mM isopropyl-β-D-thiogalactoside (IPTG) overnight at 25 °C, cells were lysed and PKA-C purified using STREP-Tactin Superflow column (IBA Lifesciences) chromatography, following the manufacturer's instructions. The obtained rPKA-C was stored at 4 °C and was used for biochemical and electrophysiological experiments within 1 to 2 wk. Significant loss of catalytic activity and efficiency toward CFTR became apparent after 5 to 6 wk of storage. For coexpression of *C. parvum* NMT with recombinant bovine PKA-C, pJ411-PKA-C and pET14b-NMT were cotransformed into *E. coli* Rosetta 2(DE3) cells Merck (Millipore) and PKA-C purified as described above (*SI Appendix*, Fig. S1*B*, *brown chromatograms*; *SI Appendix*, Fig. S1 *C*, *Right*). For expression and purification of IpaJ and PsIpaJ, pJ411-IpaJ or pJ411-PsIpaJ was transformed into *E. coli* BL21(DE3), cells were induced with 0.5 mM IPTG overnight at 20 °C, and the proteins were purified on a STREP-Tactin Superflow column (IBA Lifesciences). IpaJ was clean without further purification as verified by size exclusion chromatography (SEC) (*SI Appendix*, Fig. S4*A*, *blue chromatogram*), whereas PsIpaJ was further purified by SEC on a Superdex 200 column (*SI Appendix*, Fig. S4*A*, *red chromatogram*). The quality of both proteins was verified by SDS-PAGE (*SI Appendix*, Fig. S4*B*).

**IpaJ and PsIpaJ Treatment of Native Bovine PKA-C.** Native bovine PKA-C (in phosphate buffer) was mixed at a 20:1 molar ratio with IpaJ or at a 5:1 molar ratio with PsIpaJ and incubated at 37 °C for 3 h or at 25 °C overnight, respectively. The protease was removed using STREP-Tactin Sepharose (IBA Lifesciences) resin (*SI Appendix*, Fig. S4 *C* and *D*).

**Kemptide Phosphorylation Assay.** Phosphorylation of the soluble substrate TAMRA-kemptide (Addexbio Technologies) was done as described (23), and dephospho- vs. phospho-kemptide were separated on TLC sheets, and their relative amounts quantitated by densitometry (ImageJ).

**Estimation of $K_I$ Values for PKI Peptides.** Expected fractional inhibition of kemptide phosphorylation by PKI(6-22)amide and PKI(14-22)amide and actual $K_I$ values under our experimental conditions were calculated as described in *SI Materials and Methods*.

**PKA-C N-Terminal Peptide Myristoylation/Demyristoylation Assay.** In vitro myristoylation of PKA-C N-terminal peptide (nonmyr-peptide) and demyristoylation of myristoylated PKA-C N-terminal peptide (myr-peptide) were done using approaches described previously (refs. 31, and 33, respectively).

**LC–MS/MS Data Acquisition and Analysis.** LC–MS/MS measurements were done by the Proteomics Core Facility unit of EMBL Heidelberg (60), as described in *SI Appendix, SI Materials and Methods*.

**Electrophysiology.** Inside-out patch-clamp recordings were performed as described (23), in a continuously flowing high-chloride bath solution, at a membrane potential of −40 mV, at 25 °C.

**Data Analysis and Statistics.** Mean steady-state currents under various test conditions were normalized to the mean current observed in the presence of 2 mM ATP + 300 nM bPKA-C in the same patch. Half-times for current activation ($t_{1/2}$) were estimated as the time required for reaching 50% of the final, steady-state current amplitude. Myristoylation stoichiometry of rPKA-C/NMT was estimated as described in *SI Appendix, SI Materials and Methods*.

Data are presented as mean ± SEM, with the number of experiments indicated in each figure legend. Significances were evaluated using Student's *t* test.

**Data, Materials, and Software Availability.** All study data are included in the article and/or *SI Appendix*.

**ACKNOWLEDGMENTS.** We thank Alexandra Reers and Robin Prentice (Seattle Structural Genomics Center for Infectious Disease) for providing the coding sequence for *Cryptosporidium parvum* NMT and purified NMT protein and Dr. Angus Nairn (Yale University) for expert advice on bPKA-C preparation. This study was supported by European Union Horizon 2020 Research and Innovation Program Grant 739593 and Cystic Fibrosis Foundation Research Grant CSANAD21G0 to L.C., as well as by National Research, Development and Innovation Office Grants KKP 144199 to L.C. and PD 131643 to C.M.

Author affiliations: [a]Department of Biochemistry, Semmelweis University, Budapest H-1094, Hungary; [b]Molecular Channelopathies Research Group, Hungarian Centre of Excellence for Molecular Medicine - Semmelweis University, Budapest H-1094, Hungary; and [c]Ion Channel Research Group, Hungarian Research Network - Semmelweis University, Budapest H-1094, Hungary

1. M. C. Rao, Physiology of electrolyte transport in the gut: Implications for disease. *Comp. Physiol.* **9**, 947–1023 (2019).
2. F. Jouret, O. Devuyst, Targeting chloride transport in autosomal dominant polycystic kidney disease. *Cell Signal.* **73**, 109703 (2020).
3. V. E. Torres *et al.*, Tolvaptan in patients with autosomal dominant polycystic kidney disease. *N. Engl. J. Med.* **367**, 2407–2418 (2012).
4. F. Wang, S. Zeltwanger, S. Hu, T. C. Hwang, Deletion of phenylalanine 508 causes attenuated phosphorylation-dependent activation of CFTR chloride channels. *J. Physiol.* **524**, 637–648 (2000).
5. W. Wang *et al.*, G551D mutation impairs PKA-dependent activation of CFTR channel that can be restored by novel GOF mutations. *Am. J. Physiol. Lung Cell Mol. Physiol.* **319**, L770–L785 (2020).
6. P. J. Barry *et al.*, Triple Therapy for cystic fibrosis Phe508del-gating and -residual function genotypes. *N. Engl. J. Med.* **385**, 815–825 (2021).
7. F. Van Goor *et al.*, Rescue of CF airway epithelial cell function in vitro by a CFTR potentiator, VX-770. *Proc. Natl. Acad. Sci. U.S.A.* **106**, 18825–18830 (2009).
8. S. T. Pallenberg *et al.*, Impact of elexacaftor/tezacaftor/ivacaftor therapy on the cystic fibrosis airway microbial metagenome. *Microbiol. Spectr.* **10**, e0145422 (2022).
9. J. R. Riordan *et al.*, Identification of the cystic fibrosis gene: Cloning and characterization of complementary DNA. *Science* **245**, 1066–1073 (1989).
10. P. Vergani, S. W. Lockless, A. C. Nairn, D. C. Gadsby, CFTR channel opening by ATP-driven tight dimerization of its nucleotide-binding domains. *Nature* **433**, 876–880 (2005).
11. K. L. Gunderson, R. R. Kopito, Conformational states of CFTR associated with channel gating: The role ATP binding and hydrolysis. *Cell* **82**, 231–239 (1995).
12. L. Csanády, P. Vergani, D. C. Gadsby, Strict coupling between CFTR's catalytic cycle and gating of its $Cl^-$ ion pore revealed by distributions of open channel burst durations. *Proc. Natl. Acad. Sci. U.S.A.* **107**, 1241–1246 (2010).
13. S. H. Cheng *et al.*, Phosphorylation of the R domain by cAMP-dependent protein kinase regulates the CFTR chloride channel. *Cell* **66**, 1027–1036 (1991).
14. D. P. Rich *et al.*, Effect of deleting the R domain on CFTR-generated chloride channels. *Science* **253**, 205–207 (1991).
15. R. E. Turnham, J. D. Scott, Protein kinase A catalytic subunit isoform PRKACA: History, function and physiology. *Gene* **577**, 101–108 (2016).
16. S. A. Carr, K. Biemann, S. Shoji, D. C. Parmelee, K. Titani, n-Tetradecanoyl is the NH2-terminal blocking group of the catalytic subunit of cyclic AMP-dependent protein kinase from bovine cardiac muscle. *Proc. Natl. Acad. Sci. U.S.A.* **79**, 6128–6131 (1982).
17. J. Toner-Webb, S. M. van Patten, D. A. Walsh, S. S. Taylor, Autophosphorylation of the catalytic subunit of cAMP-dependent protein kinase. *J. Biol. Chem.* **267**, 25174–25180 (1992).
18. L. S. Ostedgaard, O. Baldursson, D. W. Vermeer, M. J. Welsh, A. D. Robertson, A functional R domain from cystic fibrosis transmembrane conductance regulator is predominantly unstructured in solution. *Proc. Natl. Acad. Sci. U.S.A.* **97**, 5657–5662 (2000).
19. Z. Zhang, J. Chen, Atomic structure of the cystic fibrosis transmembrane conductance regulator. *Cell* **167**, 1586–1597 (2016).
20. F. Liu, Z. Zhang, L. Csanády, D. C. Gadsby, J. Chen, Molecular structure of the human CFTR ion channel. *Cell* **169**, 85–95 (2017).
21. Z. Zhang, F. Liu, J. Chen, Conformational changes of CFTR upon phosphorylation and ATP binding. *Cell* **170**, 483–491 (2017).
22. Z. Zhang, F. Liu, J. Chen, Molecular structure of the ATP-bound, phosphorylated human CFTR. *Proc. Natl. Acad. Sci. U.S.A.* **115**, 12757–12762 (2018).
23. C. Mihályi, I. Iordanov, B. Torocsik, L. Csanády, Simple binding of protein kinase A prior to phosphorylation allows CFTR anion channels to be opened by nucleotides. *Proc. Natl. Acad. Sci. U.S.A.* **117**, 21740–21746 (2020).
24. J. G. Demaille, K. A. Peters, E. H. Fischer, Isolation and properties of the rabbit skeletal muscle protein inhibitor of adenosine 3′, 5′-monophosphate dependent protein kinases. *Biochemistry* **16**, 3080–3086 (1977).
25. D. B. Glass, H. C. Cheng, L. Mende-Mueller, J. Reed, D. A. Walsh, Primary structural determinants essential for potent inhibition of cAMP-dependent protein kinase by inhibitory peptides corresponding to the active portion of the heat-stable inhibitor protein. *J. Biol. Chem.* **264**, 8802–8810 (1989).
26. L. K. Kaczmarek *et al.*, Microinjection of catalytic subunit of cyclic AMP-dependent protein kinase enhances calcium action potentials of bag cell neurons in cell culture. *Proc. Natl. Acad. Sci. U.S.A.* **77**, 7487–7491 (1980).
27. K. Viht, A. Vaasa, G. Raidaru, E. Enkvist, A. Uri, Fluorometric TLC assay for evaluation of protein kinase inhibitors. *Anal. Biochem.* **340**, 165–170 (2005).
28. W. Yonemoto, S. M. Garrod, S. M. Bell, S. S. Taylor, Identification of phosphorylation sites in the recombinant catalytic subunit of cAMP-dependent protein kinase. *J. Biol. Chem.* **268**, 18626–18632 (1993).
29. L. Csanády, B. Torocsik, Cystic fibrosis drug ivacaftor stimulates CFTR channels at picomolar concentrations. *eLife* **8**, e46450 (2019).
30. L. W. Slice, S. S. Taylor, Expression of the catalytic subunit of cAMP-dependent protein kinase in *Escherichia coli*. *J. Biol. Chem.* **264**, 20940–20946 (1989).
31. N. Burnaevskiy *et al.*, Proteolytic elimination of N-myristoyl modifications by the *Shigella* virulence factor IpaJ. *Nature* **496**, 106–109 (2013).
32. R. J. Duronio *et al.*, Protein N-myristoylation in *Escherichia coli*: Reconstitution of a eukaryotic protein modification in bacteria. *Proc. Natl. Acad. Sci. U.S.A.* **87**, 1506–1510 (1990).
33. E. C. Gaffarogullari *et al.*, A myristoyl/phosphoserine switch controls cAMP-dependent protein kinase association to membranes. *J. Mol. Biol.* **411**, 823–836 (2011).
34. A. C. Bastidas *et al.*, Role of N-terminal myristylation in the structure and regulation of cAMP-dependent protein kinase. *J. Mol. Biol.* **422**, 215–229 (2012).
35. W. Yonemoto, M. L. McGlone, B. Grant, S. S. Taylor, Autophosphorylation of the catalytic subunit of cAMP-dependent protein kinase in *Escherichia coli*. *Protein Eng.* **10**, 915–925 (1997).
36. S. Depluverez, S. Devos, B. Devreese, The role of bacterial secretion systems in the virulence of gram-negative airway pathogens associated with cystic fibrosis. *Front. Microbiol.* **7**, 1336 (2016).
37. N. Burnaevskiy, T. Peng, L. E. Reddick, H. C. Hang, N. M. Alto, Myristoylome profiling reveals a concerted mechanism of ARF GTPase deacylation by the bacterial protease IpaJ. *Mol. Cell* **58**, 110–122 (2015).
38. J. D. Scott, M. B. Glaccum, E. H. Fischer, E. G. Krebs, Primary-structure requirements for inhibition by the heat-stable inhibitor of the cAMP-dependent protein kinase. *Proc. Natl. Acad. Sci. U.S.A.* **83**, 1613–1616 (1986).
39. G. A. Olah, R. D. Mitchell, T. R. Sosnick, D. A. Walsh, J. Trewhella, Solution structure of the cAMP-dependent protein kinase catalytic subunit and its contraction upon binding the protein kinase inhibitor peptide. *Biochemistry* **32**, 3649–3657 (1993).
40. S. S. Taylor *et al.*, PKA: A portrait of protein kinase dynamics. *Biochim. Biophys. Acta* **1697**, 259–269 (2004).
41. L. R. Masterson, A. Cembran, L. Shi, G. Veglia, Allostery and binding cooperativity of the catalytic subunit of protein kinase A by NMR spectroscopy and molecular dynamics simulations. *Adv. Protein Chem. Struct. Biol.* **87**, 363–389 (2012).
42. P. Zhang *et al.*, Structure and allostery of the PKA RIIbeta tetrameric holoenzyme. *Science* **335**, 712–716 (2012).
43. O. Haji-Ghassemi, Z. Yuchi, F. Van Petegem, The cardiac ryanodine receptor phosphorylation hotspot embraces PKA in a phosphorylation-dependent manner. *Mol. Cell* **75**, 39–52 (2019).
44. J. Qin *et al.*, Structures of PKA-phospholamban complexes reveal a mechanism of familial dilated cardiomyopathy. *eLife* **11**, e75346 (2022).
45. M. R. Picciotto, J. A. Cohn, G. Bertuzzi, P. Greengard, A. C. Nairn, Phosphorylation of the cystic fibrosis transmembrane conductance regulator. *J. Biol. Chem.* **267**, 12742–12752 (1992).
46. O. Zetterqvist, U. Ragnarsson, E. Humble, L. Berglund, L. Engström, The minimum substrate of cyclic AMP-stimulated protein kinase, as studied by synthetic peptides representing the phosphorylatable site of pyruvate kinase (type L) of rat liver. *Biochem. Biophys. Res. Commun.* **70**, 696–703 (1976).
47. B. E. Kemp, D. J. Graves, E. Benjamini, E. G. Krebs, Role of multiple basic residues in determining the substrate specificity of cyclic AMP-dependent protein kinase. *J. Biol. Chem.* **252**, 4888–4894 (1977).
48. W. Yonemoto, M. L. McGlone, S. S. Taylor, N-myristylation of the catalytic subunit of cAMP-dependent protein kinase conveys structural stability. *J. Biol. Chem.* **268**, 2348–2352 (1993).
49. C. H. Clegg, W. Ran, M. D. Uhler, G. S. McKnight, A mutation in the catalytic subunit of protein kinase A prevents myristylation but does not inhibit biological activity. *J. Biol. Chem.* **264**, 20140–20146 (1989).
50. J. L. Meinkoth, Y. Ji, S. S. Taylor, J. R. Feramisco, Dynamics of the distribution of cyclic AMP-dependent protein kinase in living cells. *Proc. Natl. Acad. Sci. U.S.A.* **87**, 9595–9599 (1990).
51. S. S. Taylor, R. Ilouz, P. Zhang, A. P. Kornev, Assembly of allosteric macromolecular switches: Lessons from PKA. *Nat. Rev. Mol. Cell Biol.* **13**, 646–658 (2012).
52. M. G. Gold, Swimming regulations for protein kinase A catalytic subunit. *Biochem. Soc. Trans.* **47**, 1355–1366 (2019).
53. M. Gangal *et al.*, Mobilization of the A-kinase N-myristate through an isoform-specific intermolecular switch. *Proc. Natl. Acad. Sci. U.S.A.* **96**, 12394–12399 (1999).
54. P. Zhang *et al.*, An isoform-specific myristylation switch targets type II PKA holoenzymes to membranes. *Structure* **23**, 1563–1572 (2015).
55. S. E. Tillo *et al.*, Liberated PKA catalytic subunits associate with the membrane via myristoylation to preferentially phosphorylate membrane substrates. *Cell Rep.* **19**, 617–629 (2017).
56. J. D. Mougous *et al.*, A virulence locus of *Pseudomonas aeruginosa* encodes a protein secretion apparatus. *Science* **312**, 1526–1530 (2006).
57. C. J. Harding, M. Bischoff, M. Bergkessel, C. M. Czekster, An anti-biofilm cyclic peptide targets a secreted aminopeptidase from *P. aeruginosa*. *Nat. Chem. Biol.* **19**, 1158–1166 (2023).
58. J. M. Bomberger *et al.*, Long-distance delivery of bacterial virulence factors by *Pseudomonas aeruginosa* outer membrane vesicles. *PLoS Pathog.* **5**, e1000382 (2009).
59. M. A. Simon, L. Csanády, Molecular pathology of the R117H cystic fibrosis mutation is explained by loss of a hydrogen bond. *eLife* **10**, e74693 (2021).
60. H. Franken *et al.*, Thermal proteome profiling for unbiased identification of direct and indirect drug targets using multiplexed quantitative mass spectrometry. *Nat. Protoc.* **10**, 1567–1593 (2015).